

# Hybrid semiclassical theory of quantum quenches in one dimensional systems

Cătălin Paşcu Moca,<sup>1,2</sup> Márton Kormos,<sup>3</sup> and Gergely Zaránd<sup>1</sup>

<sup>1</sup>*BME-MTA Exotic Quantum Phase Group, Institute of Physics, Budapest University of Technology and Economics, H-1111 Budapest, Hungary*

<sup>2</sup>*Department of Physics, University of Oradea, 410087, Oradea, Romania*

<sup>3</sup>*BME-MTA Statistical Field Theory Research Group, Institute of Physics, Budapest University of Technology and Economics, H-1111 Budapest, Hungary*

(Dated: January 25, 2022)

We develop a hybrid semiclassical method to study the time evolution of one dimensional quantum systems in and out of equilibrium. Our method handles internal degrees of freedom completely quantum mechanically by a modified time evolving block decimation method, while treating orbital quasiparticle motion classically. We can follow dynamics up to timescales well beyond the reach of standard numerical methods to observe the crossover between pre-equilibrated and locally phase equilibrated states. As an application, we investigate the quench dynamics and phase fluctuations of a pair of tunnel coupled one dimensional Bose condensates. We demonstrate the emergence of soliton-collision induced phase propagation, soliton-entropy production and multistep thermalization. Our method can be applied to a wide range of gapped one-dimensional systems.

Fundamental questions concerning the coherent time evolution, relaxation and thermalization of isolated quantum systems have been brought into the focus of attention by recent progress in experimental techniques [1–4]. Experiments on cold atomic gases allow us to engineer a broad range of lattice and continuum Hamiltonians in a controlled fashion, and to monitor the coherent time evolution of these systems through measuring multi-point correlation functions [5], accessing the quantum state via site-resolved quantum microscopy [6], and even measuring the entanglement properties of the system [7]. These experiments as well as ongoing matter wave interferometry [8] experiments call for the development of new analytical and numerical methods that are able to describe non-equilibrium dynamics in closed interacting quantum systems, and address fundamental questions of non-equilibrium thermodynamics, such as thermalization, entropy production, or the fate of pre-thermalized states.

Here we propose a novel method we dub “semi-semiclassical” (sSC), able to reach time scales much beyond conventional methods [9–11] and to capture the fundamental phenomena of pre-thermalization [12, 13] as well as local equilibration in great detail. Our method hybridizes a semiclassical (SC) approach with time-evolving block decimation (TEBD): we compute the time evolution of the internal degrees of freedom completely quantum mechanically using TEBD, while treating the orbital motion semiclassically. As a proof of principle, we use our method to describe quantum quenches in the sine-Gordon model, relevant for two coupled 1D quasicondensates (see Fig. 1.b), and studied intensely both theoretically [14–18] and in matter wave interference experiments using nanofabricated atom chips [3, 19]. Our sSC method is demonstrated to capture multistep thermalization and soliton-collision induced entropy production efficiently, and is applicable to one dimensional gapped systems hav-

ing stable quasiparticle excitations [20].

Our method is based on a semiclassical (SC) approach, originally developed to study the dynamics of finite temperature systems in equilibrium [21–23] and later successfully applied to quantum quenches [24–27], i.e. to non-equilibrium situations in which the system evolves unitarily starting from some prepared initial state. The SC method is applicable in gapped systems whenever the quasiparticles’ Compton wavelength (or the thermal wavelength) is much shorter than their average separation,  $d = \rho^{-1}$ , with  $\rho$  the quasiparticle density. If the energy of the initial state is not too high, it acts as a weak source of almost pointlike quasiparticles, following clas-

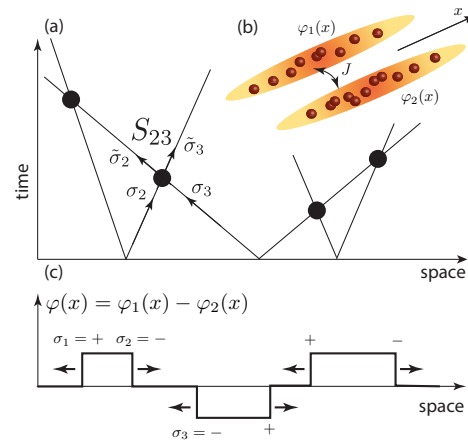


FIG. 1. (Color online) (a) Space-time diagram of quasiparticle trajectories. Labels  $\sigma = \pm$  represent internal soliton/antisoliton quantum numbers. Collisions are described by the quantum mechanical  $S$ -matrix (solid black dot). (b) One dimensional Bose condensates coupled by quantum tunneling. Dynamics of the relative phase is described by the sine-Gordon model. (c) The quench creates soliton-antisoliton pairs at  $t = 0$ . Arrows indicate directions of propagation.

sical trajectories [28, 29] (see Fig. 1.a). In the standard SC treatment, quasiparticles are furthermore assumed to move slowly and thus collisions are described by a universal purely reflective scattering matrix [30]. This universal SC (uSC) approach permits the derivation of precious analytical results [22, 23, 26, 27], but also suffers from artifacts [23, 27]; certain correlation functions and expectation values fail to decay and internal degrees of freedom remain just locally entangled. Our method eliminates all these shortcomings [31].

*Model.*— The sine-Gordon model is defined as

$$H = \frac{\hbar c}{2} \int dx \left[ \frac{2\pi}{K} \Pi(x)^2 + \frac{K}{2\pi} [\partial_x \varphi(x)]^2 \right] - \int dx 2\Delta_0 \cos[\varphi(x)], \quad (1)$$

with  $\Pi(x)$  denoting the field conjugate to  $\varphi(x)$ , and  $c$  the speed of sound. In case of coupled condensates,  $\varphi(x) = \varphi_1(x) - \varphi_2(x)$  represents the relative phase of the condensates,  $K$  stands for the Luttinger parameter of each condensate, and the cosine term accounts for Josephson tunneling between them [32]. For locally interacting bosons  $K \geq 1$ , with  $K \gg 1$  corresponding to weak interactions. The cosine perturbation is relevant for  $K > 1/4$ , and for  $K < 1/2$  there are only kink excitations in the system, solitons and antisolitons. In the classical field theory, these kinks interpolate between neighboring minima of the cosine potential and have topological charges  $\sigma = \pm$  corresponding to changes  $\varphi \rightarrow \varphi \pm 2\pi$ , respectively. For  $K > 1/2$  their bound states, the so-called breathers are also present. However, having no topological charge, breathers are supposed to be irrelevant for the long time (large distance) phase correlations studied here, and shall therefore be neglected in what follows.

We illustrate our method on the out of equilibrium time evolution of the coupled 1D condensates after changing the potential barrier that separates them. For small changes in the model parameters the quench is perturbative, and the gas of quasiparticles (kinks) created in the quench will be dilute such that the SC method can be applied [24, 33]. Furthermore, by momentum conservation, a homogeneous but spatially localized perturbation gives rise to pairs of kinks flying away from each other with the same velocity and opposite topological charge. Thus the post-quench state will be populated by independent soliton-antisoliton pairs created with a velocity distribution  $f(v)$ . The precise form of  $f(v)$  depends on details of the quench protocol, but turns out to be unimportant in the present calculation. The initial state considered here resembles to the ones appearing in previous studies of split condensates [34, 35] as well as other systems [16, 36–41], where the initial state was taken to be a coherent superposition of uncorrelated zero momentum quasiparticle pairs. Within our sSC approach, however, phase coherence of the pairs does not play any role.

*The semi-semiclassical (sSC) method.*— In the SC approach, the quantum mechanical average is replaced by an ensemble average over initial positions and velocities of soliton-antisoliton pairs. The corresponding semiclassical configurations consist of space-time diagrams with pairs of straight lines (kink trajectories) originating from the  $t = 0$  axis, distributed independently from each other, uniformly in space with random slopes corresponding to the distribution  $f(v)$  (see Fig. 1.a), and an initial distribution of paired charges.

Since quantum mechanical effects become relevant only at collisions, we can approximately factorize the many body wave function into an orbital and a charge part of the form  $|\Psi(\mathbf{x}, \boldsymbol{\sigma}, t)\rangle \approx \mathcal{S}|\Psi_{\text{orb}}(\mathbf{x}, t)\rangle \otimes |\chi(\boldsymbol{\sigma}, t)\rangle$ , where

$$|\Psi_{\text{orb}}(\mathbf{x}, t)\rangle = \int d^N x \prod_{j=1}^N \delta(x_j - x_j^0 - v_j t) |x_1, \dots, x_N\rangle, \\ |\chi(\boldsymbol{\sigma}, t)\rangle = \sum_{\sigma_1, \sigma_2, \dots} \mathcal{A}_{\sigma_1 \sigma_2 \dots \sigma_N} |\sigma_1 \sigma_2 \dots \sigma_N\rangle. \quad (2)$$

Here  $x_j^0$  denotes the initial position of the  $j^{\text{th}}$  kink of velocity  $v_j$  and topological charge  $\sigma_j$ , and  $\mathcal{S}$  stands for symmetrization.

In the original uSC approach charges are treated classically: quasiparticles scatter as impenetrable billiard balls while preserving their charges. This follows from the perfectly reflective universal low energy two-body  $S$ -matrix,  $S_{\sigma_1 \sigma_2}^{\tilde{\sigma}_1 \tilde{\sigma}_2} = (-1)^{\delta_{\sigma_1 \tilde{\sigma}_1} \delta_{\sigma_2 \tilde{\sigma}_2}}$  (notice the labeling convention), describing the scattering of quasiparticles with vanishing momenta. Using this perfectly reflective  $S$ -matrix allows one to obtain a number of exact results for thermal gases and near adiabatic quantum quenches [22, 23, 26, 27]. However, as soon as the quench is not slow enough, faster quasiparticles are inevitably created. Collisions involving these faster particles are not captured by the universal scattering matrix, and the true velocity dependent scattering matrix must be used (cf. Fig. 1.a). The sine-Gordon model is integrable and this two-particle  $S$ -matrix is exactly known [42, 43]. The matrix elements  $S_{+-}^{\pm-} = S_{\text{R}}(v_1, v_2)$  and  $S_{+-}^{-+} = S_{\text{T}}(v_1, v_2)$ , in particular, describe reflection and transmission, respectively. They satisfy  $|S_{\text{T}}|^2 + |S_{\text{R}}|^2 = 1$ , and for small velocities transmission vanishes as  $|S_{\text{T}}(v_1, v_2)|^2 \propto (v_1 - v_2)^2$ .

We can incorporate the non-trivial  $S$ -matrix in two different ways. In the first method, charges are still treated classically, but at each collision either a perfect transmission or perfect reflection takes place with probabilities given by the modulus square of the  $S$ -matrix elements. This method neglects interference effects but can be implemented as a classical Monte-Carlo simulation. A more refined approach is to treat the charge part of the wave function in Eq. (2) in a fully quantum mechanical manner with an MPS-based method. As the quench protocol generates neutral kink pairs with equal probability amplitude, the initial wave function is a dimerized state, i.e.

a product of Bell pairs:

$$|\chi(\boldsymbol{\sigma}, t = 0)\rangle = \prod_{j=1}^{N/2} \frac{|+\rangle_{2j-1} |-\rangle_{2j} + |-\rangle_{2j-1} |+\rangle_{2j}}{\sqrt{2}}. \quad (3)$$

The charge wave function evolves only through collisions and it is frozen between collisions. If line  $j$  and  $j + 1$  intersect at time  $t_k$ , the change of the wave function is

$$|\chi(\boldsymbol{\sigma}, t_{k,+})\rangle = \hat{S}_{j,j+1}(t_k) |\chi(\boldsymbol{\sigma}, t_{k,-})\rangle, \quad (4)$$

where  $\hat{S}_{j,j+1}(t_k)$  acts nontrivially only on charges  $j$  and  $j + 1$  via the 2-body  $S$ -matrix evaluated at the velocities of the colliding quasiparticles. In this way we mapped the dynamics of the charges to that of an effective quantum spin chain. The time evolution operator of this spin chain depends on the underlying semiclassical trajectories and is given as a product of local unitary two-body operators, efficiently treated by an MPS-based algorithm.

*Phase distribution.*— The space resolved relative phase  $\varphi(x)$  of the condensates can be measured directly via interferometry experiments [3, 5, 19, 44]. We first use the classical Monte Carlo approach to determine the full phase distribution after the quench, a quantity also analyzed experimentally [5], in the experiment of Ref. [5]. Semiclassically, each kink is a domain wall that separates two domains with a phase difference of  $\pm 2\pi$ . Domains separated by  $s$  kinks have a phase difference  $\Delta\varphi = 2\pi \sum_{i=1}^s \sigma_i$ . The phase in a given domain being constant, its distribution function is a sum of weighted Dirac-delta peaks located at integer multiples of  $2\pi$ ,

$$P(\varphi, t) = \sum_{n \in \mathbb{Z}} c_{2\pi n}(t) \delta(\varphi - 2\pi n). \quad (5)$$

In experiments, these delta peaks get broadened by quantum and thermal fluctuations. To take this into account, we estimated the phase fluctuations  $\langle \varphi(x)^2 \rangle$  around the minima of the cosine potential for typical parameters [43], and broadened the delta-functions accordingly.

The resulting phase distribution  $P(\varphi, t)$  is shown in Fig. 2.a at different instances for a typical small quench. For the momentum distribution of quasiparticles,  $f(p)$ , we used the ansatz  $f(p) \propto p^2 \exp(-p^2/p_0^2)$ , motivated by overlap expressions in the transverse field Ising model [45]. Immediately after the quench, there is a single central peak at  $\varphi = 0$  and  $c_0(0) = 1$ , but side peaks emerge as the system evolves in time. The two side peaks at  $\varphi = \pm 2\pi$  emerge already at the uSC level: initially, domains of phase  $\varphi = \pm 2\pi$  grow ballistically between separating soliton-antisoliton pairs (see Fig. 1.c), therefore  $c_0$  decreases while  $c_{\pm 2\pi}$  increase linearly in time. Within the uSC approach, the weights  $c_{\pm 2\pi}$  saturate at  $c_{\pm 2\pi} \rightarrow 1/4$  once the coordinates of the kinks become randomized, while the central peak levels off at  $c_0 \rightarrow 1/2$ . We observe this ‘pre-thermalized’ behavior by sSC at intermediate times in simulations with small quasiparticle

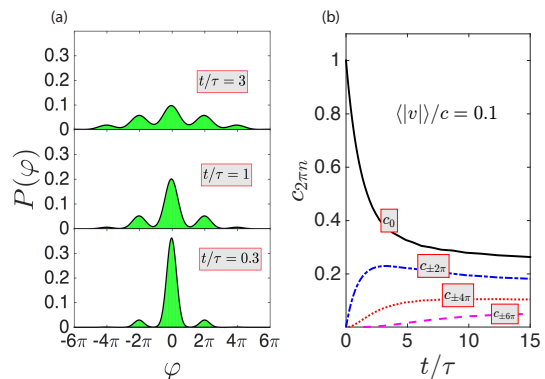


FIG. 2. (a) Phase distributions  $P(\varphi, t)$  at different times for a system of  $N = 24$  kinks with  $\langle |v| \rangle = 0.1c$  and Luttinger parameter  $K = 9.82$ . (b) Time dependence of the weights  $c_{2\pi n}$  defined in Eq. (5).

velocities  $\langle |v| \rangle / c \lesssim 0.05$ . However, after a fast relaxation, collisions start to dominate beyond the collision time,  $t \gtrsim \tau = \rho \int_0^\infty dv v f(v)$ , and *phase propagation* takes place due to transmissive collisions, giving rise to domains of phases  $\varphi = \pm 4\pi, \pm 6\pi, \dots$ , and the emergence of further side peaks (see Fig. 2.b). These are all expected to vanish as  $c_{2\pi n} \sim 1/\sqrt{t}$  for very long times, reflecting the expected diffusive nature of phase propagation, as indeed supported by our numerical results (see [43]).

*Entanglement entropy.*— Our method is able to follow the propagation and growth of entanglement in the charge sector. The most widely used entanglement measure is the entanglement entropy of a subsystem  $A$ , defined as the von Neumann entropy of its reduced density matrix:  $S = -\text{Tr}_A[\rho_A \log \rho_A]$  where  $\rho_A = \text{Tr}_{\bar{A}} |\Psi(\mathbf{x}, \boldsymbol{\sigma}, t)\rangle \langle \Psi(\mathbf{x}, \boldsymbol{\sigma}, t)|$ . Here we focus on the simple case when  $A$  is half of the total system. The initial charge wave function  $|\chi\rangle$  has alternating bond entanglement entropies of  $\log 2$  and 0. At  $t = 0^+$ , the spatial extension of the entangled bonds is zero, so with probability 1 the cut between the two halves of the system falls between entangled pairs resulting in zero entanglement entropy. Within the uSC approximation, at  $t > 0$ , pairs with one member on the left and another member on the right entangle the two halves of the system. Since the uSC  $S$ -matrix is fully reflective, each kink remains maximally entangled with its original partner, but entanglement remains local. At very long times, the cut between the two halves of the system either falls between pairs or cuts a pair in two with probability 1/2. Consequently, the entanglement entropy saturates at a value  $S_{\text{sat}} = \log 2/2$ . The full time evolution of the entropy is simple to calculate within the uSC approach which yields an exponential relaxation to  $S_{\text{sat}}$ ,  $S_{\text{uSC}}(t) = (1 - e^{-t/\tau}) \ln 2/2$ , (solid black line in Fig. 3). The saturation of  $S_{\text{uSC}}(t)$  is clearly an artefact of the uSC method. In reality, the topological charges of remote quasiparticles become entangled with time due to trans-

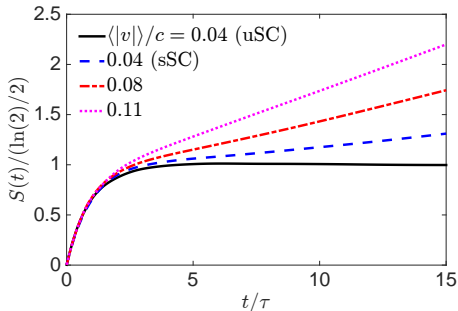


FIG. 3. Dynamics of charge entanglement entropy after the quench for the same parameters as in Fig. 2. The solid black line denotes the uSC result with a fully reflective  $S$ -matrix.

missive scattering processes. The sSC approach captures the corresponding entropy production: the entanglement entropy does not saturate after the initial transient, but is found to grow *linearly* in time without bound in an infinite system,  $S(t) = \alpha t$ , with a growth rate  $\alpha \propto \langle |v| \rangle$ .

*Correlation functions and equilibration.*— The sSC method is also suitable for computing the out of equilibrium evolution of correlation functions. We consider first the expectation values  $G_\alpha(t) = \langle e^{i\alpha\varphi(x,t)} \rangle = \langle e^{i\alpha\varphi(x,t)} e^{-i\alpha\varphi(x,0)} \rangle$ . The function  $G_1(t)$  is essentially the coherence factor, directly accessible through matter wave interferometry [3]. The standard uSC approach has been recently used to compute  $G_\alpha(t)$  [27], which was found to decay exponentially to a value  $\cos^2(\pi\alpha)$ , apart from a prefactor incorporating vacuum fluctuations, now set to one (see Fig. 4.a). This surprising behavior is related to the fact that in the uSC approach the phase is pinned to the values  $\varphi = 0, \pm 2\pi$ . In contrast, within the sSC approach, the phase meanders with time and  $G_\alpha(t \rightarrow \infty)$  no longer remains finite; after a fast transient described approximately by uSC,  $G_\alpha(t)$  is found to decay exponentially to zero with a rate depending on  $\langle |v| \rangle / c$ . The equal time two-point correlation functions,

$$C_\alpha(x - x'; t) = \langle e^{i\alpha\varphi(x,t)} e^{-i\alpha\varphi(x',t)} \rangle, \quad (6)$$

are also accessible experimentally [46], and the integrated quantity,  $\int dx dx' C_1(x - x'; t)$ , is directly related to the contrast of the interference fringes. Fig. 4.b shows the time evolution of  $C_\alpha(x; t)$  for  $\alpha = 1/2$ . Here again, the uSC approach yields a quick relaxation to a state, where the phase is pinned and, accordingly, long-ranged correlations persist,  $C_\alpha(|x|, t \rightarrow \infty) \sim \cos^4(\pi\alpha)$ .

In sharp contrast to traditional uSC, within the sSC we find that  $C_\alpha(x - x', \infty) = \exp(-2 \sin^2(\pi\alpha)\rho|x - x'|)$  which formally coincides with the *thermal* equilibrium correlator computed within the standard finite temperature SC approach [22]. In our case, however, the final state is *not* thermal: in the spirit of Generalized Gibbs Ensemble (GGE) the density  $\rho$  is conserved and set by

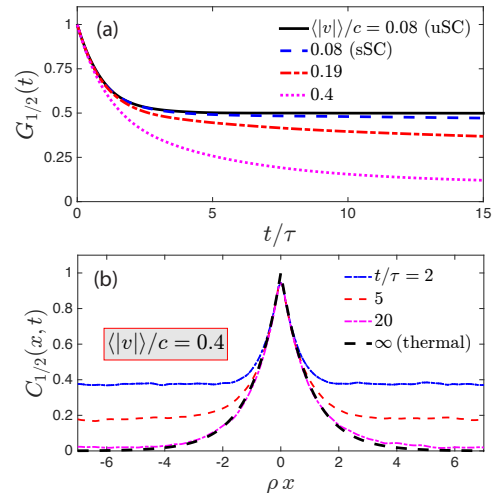


FIG. 4. (a) Relaxation of the expectation value  $\langle e^{i\varphi(x,t)/2} \rangle$  for different average velocities. The solid black line represents the uSC result (fully reflective  $S$ -matrix). (b) Equal time correlation function  $\langle e^{i\varphi(x,t)/2} e^{-i\varphi(x',t)/2} \rangle$  at different times calculated with the sSC method. The black dashed line is the thermal equilibrium result in the uSC approximation.

the initial state rather than a single effective temperature [47]. The final state we obtain should rather be viewed as a *pre-thermalized* state, where local phase correlations and expectation values of vertex operators look thermal, but the velocity distribution of the quasiparticles remains non-thermal, and the quasiparticles' average energy is not related to their density. The sSC method thus apparently captures aspects of local phase equilibration and “pre-thermalization”.

Equilibration is thus predicted to take place in several steps in a split condensate. For small values of  $\langle |v| \rangle / c$ , first a quick relaxation occurs to a first pre-equilibrated state with pinned phase and a non-thermal quasiparticle velocity distribution, but with kink positions randomized. Next, the coherent evolution of the charge wave function gives rise to phase (quantum) propagation. At this stage, phase correlation functions relax to their GGE values. To reach a truly thermal state with thermal quasiparticle velocity distribution a further relaxation step and coupling to some external environment such as the symmetrical phase mode are ultimately needed in the coupled condensate experiment.

*Conclusions.*— The versatile semi-semiclassical method developed here has a broad range of applicability. It is suitable for studying the dynamics of lattice systems and spin chains [33] as well as continuum 1D systems. The differences between these translate into differences in the nature of quasiparticles and their 2-body  $S$ -matrix, which makes our method ideal for identifying universal aspects of the dynamics. The semiclassical aspect allows for heuristic interpretations and relatively

long simulation times, while the quantum description of the scattering of quasiparticles allows us to go beyond the limitations of the standard uSC approach and opens the way to study the propagation of entanglement. Possible connections with the recent work [48] would be interesting to analyze. Although here we focused on the non-equilibrium time evolution, the method can also be used to investigate dynamical correlation functions at finite temperature beyond the uSC approximation, and is well-suited to study non-equilibrium dynamics in inhomogeneous 1D systems [49].

*Acknowledgements.* We thank Jörg Schmiedmayer, Eugene Demler and Ehud Altman for fruitful discussions. This work was supported by the Hungarian research fund OTKA under grant Nos. K105149 and SNN118028. M.K. was partially supported by a János Bolyai Scholarship and a Prémium Postdoctoral Fellowship of the HAS.

- 
- [1] A. Polkovnikov, K. Sengupta, A. Silva, and M. Vengalattore, *Rev. Mod. Phys.* **83**, 863 (2011).
- [2] T. Kinoshita, T. Wenger, and D. S. Weiss, *Nature* **440**, 900 (2006).
- [3] S. Hofferberth, I. Lesanovsky, B. Fischer, T. Schumm, and J. Schmiedmayer, *Nature* **449**, 324 (2007).
- [4] M. Gring, M. Kuhnert, T. Langen, T. Kitagawa, B. Rauer, M. Schreitl, I. Mazets, D. A. Smith, E. Demler, and J. Schmiedmayer, *Science* **337**, 1318 (2012).
- [5] T. Schweigler, V. Kasper, S. Erne, B. Rauer, T. Langen, T. Gasenzer, J. Berges, and J. Schmiedmayer, ArXiv e-prints (2015), [arXiv:1505.03126 \[cond-mat.quant-gas\]](https://arxiv.org/abs/1505.03126).
- [6] W. S. Bakr, J. I. Gillen, A. Peng, S. Fölling, and M. Greiner, *Nature* **462**, 74 (2009).
- [7] R. Islam, R. Ma, P. M. Preiss, M. Eric Tai, A. Lukin, M. Rispoli, and M. Greiner, *Nature* **528**, 77 (2015).
- [8] T. Schumm, S. Hofferberth, L. Andersson, S. Wildermuth, S. Groth, Bar, J. Schmiedmayer, and P. Kruger, *Nat. Phys.* **1**, 57 (2005).
- [9] S. R. White and A. E. Feiguin, *Phys. Rev. Lett.* **93**, 076401 (2004).
- [10] U. Schollwöck, *Annals of Physics* **326**, 96 (2011).
- [11] G. Vidal, *Phys. Rev. Lett.* **91**, 147902 (2003).
- [12] J. Berges, S. Borsányi, and C. Wetterich, *Phys. Rev. Lett.* **93**, 142002 (2004).
- [13] M. Buchhold, M. Heyl, and S. Diehl, *Phys. Rev. A* , 013601.
- [14] V. Gritsev, E. Demler, M. Lukin, and A. Polkovnikov, *Phys. Rev. Lett.* **99**, 200404 (2007).
- [15] A. Iucci and M. A. Cazalilla, *New J. Phys.* **12**, 055019 (2010).
- [16] B. Bertini, D. Schuricht, and F. H. L. Essler, *J. Stat. Mech.* , P10035 (2014).
- [17] C. Neuenhahn and F. Marquardt, *New Journal of Physics* **2015**, 125007 (2015).
- [18] G. Delfino and J. Viti, *J. Phys. A: Math. Theor.* **50**, 084004 (2017).
- [19] M. Kuhnert, R. Geiger, T. Langen, M. Gring, B. Rauer, T. Kitagawa, E. Demler, D. Adu Smith, and J. Schmiedmayer, *Phys. Rev. Lett.* **110**, 090405 (2013).
- [20] The most common methods, TEBD [11] and t-DMRG [9, 10], are both limited by finite size effects, and typically work only for short times, preceding thermalization. Quantum Monte Carlo techniques may be a promising direction (see G. Carleo et al., (2016) [arXiv:1612.06392](https://arxiv.org/abs/1612.06392)).
- [21] S. Sachdev and A. P. Young, *Phys. Rev. Lett.* **78**, 2220 (1997).
- [22] K. Damle and S. Sachdev, *Phys. Rev. Lett.* **95**, 187201 (2005).
- [23] A. Rapp and G. Zaránd, *Phys. Rev. B* **74**, 014433 (2006).
- [24] H. Rieger and F. Iglói, *Phys. Rev. B* **84**, 165117 (2011).
- [25] D. Rossini, A. Silva, G. Mussardo, and G. Santoro, *Phys. Rev. Lett.* **102**, 127204 (2009).
- [26] S. Evangelisti, *J. Stat. Mech.* , P04003 (2013).
- [27] M. Kormos and G. Zaránd, *Phys. Rev. E* **93**, 062101 (2016).
- [28] P. Calabrese and J. Cardy, *Phys. Rev. Lett.* **96**, 136801 (2006).
- [29] P. Calabrese and J. Cardy, *J. Stat. Mech.* **2005**, P04010 (2005).
- [30] S. Sachdev and K. Damle, *Phys. Rev. Lett.* **78**, 943 (1997).
- [31] We follow the nomenclature of Ref. [21]. There low density implies small quasiparticle momenta,  $p$ , and since  $p \sim \hbar$ , the limits  $p \rightarrow 0$  and  $\hbar \rightarrow 0$  are equivalent, explaining the term ‘semiclassical’. We lift the restriction to small  $p$  but require low quasiparticle density.
- [32] V. Gritsev, A. Polkovnikov, and E. Demler, *Phys. Rev. B* **75**, 174511 (2007).
- [33] Detailed iTEBD simulations on the spin  $S = 1$  Heisenberg chain validity of the sSC approach in the dilute limit [M. Werner, C.P. Moca, M. Kormos, and G. Zaránd, unpublished].
- [34] T. Kitagawa, A. Imambekov, J. Schmiedmayer, and E. Demler, *New J. Phys.* **13**, 073018 (2011).
- [35] L. Foini and T. Giamarchi, *Phys. Rev. A* **91**, 023627 (2015).
- [36] A. Silva, *Phys. Rev. Lett.* **101**, 120603 (2008).
- [37] S. Sotiriadis and J. Cardy, *Phys. Rev. B* **81**, 134305 (2010).
- [38] D. Fioretto and G. Mussardo, *New J. Phys.* **12**, 55015 (2010).
- [39] J. De Nardis, B. Wouters, M. Brockmann, and J.-S. Caux, *Phys. Rev. A* **89**, 033601 (2014).
- [40] B. Pozsgay, *J. Stat. Mech.* , P06011 (2014).
- [41] D. Horváth, S. Sotiriadis, and G. Takács, *Nucl. Phys. B* **902**, 508 (2016).
- [42] A. B. Zamolodchikov and A. B. Zamolodchikov, *Annals of Physics* **120**, 253 (1979).
- [43] C. P. Moca, M. Kormos, and G. Zaránd, [Supplementary material](#) .
- [44] G. B. Jo, J. H. Choi, C. A. Christensen, Y. R. Lee, T. A. Pasquini, W. Ketterle, and D. E. Pritchard, *Phys. Rev. Lett.* **99**, 240406 (2007).
- [45] P. Calabrese, F. H. L. Essler, and M. Fagotti, *J. Stat. Mech.* , P07016 (2012).
- [46] T. Langen, R. Geiger, M. Kuhnert, B. Rauer, and J. Schmiedmayer, *Nat. Phys.* **9**, 1 (2013).
- [47] M. Rigol, V. Dunjko, V. Yurovsky, and M. Olshanii, *Physical Review Letters* **98**, 050405 (2007).
- [48] V. Alba and P. Calabrese, (2016), [arXiv:1608.00614](https://arxiv.org/abs/1608.00614).
- [49] M. Kormos, C.P. Moca, and G. Zaránd, unpublished.
- [50] In the present calculation the velocity distribution is derived from a distribution with relativistic dispersion, but

we have checked that the results remain largely unaltered

by using different distributions.

## Supplemental Material

### The Hamiltonian and sine–Gordon description of coupled quasicondensates

The Hamiltonian of two coupled 1D condensates is given by [32]

$$H = \sum_{j=1,2} \int dx \left\{ \frac{\hbar^2}{2m} \partial_x \psi_j^\dagger(x) \partial_x \psi_j(x) + \frac{g}{2} \psi_j^\dagger(x) \psi_j^\dagger(x) \psi_j(x) \psi_j(x) + [V(x) - \mu] \psi_j^\dagger(x) \psi_j(x) \right\} - \hbar J \int dx \left[ \psi_1^\dagger(x) \psi_2(x) + \psi_2^\dagger(x) \psi_1(x) \right], \quad (\text{S-7})$$

where  $\psi_1(x), \psi_2(x)$  are the bosonic fields in the two condensates,  $V(x)$  is the longitudinal potential which we neglect in the following,  $J$  is the tunnel coupling between the condensates, and

$$g = \frac{2\hbar^2 a_s}{m l_\perp^2} \left( 1 - 1.0325 \frac{a_s}{l_\perp} \right)^{-1} \quad (\text{S-8})$$

is the strength of the atom-atom interaction within each condensate. Here  $l_\perp = \sqrt{\hbar/(m\omega_\perp)}$  with  $\omega_\perp$  being the frequency of the radial confining potential and  $a_s$  denotes the  $s$ -wave scattering length of the atoms. The strength of interaction is often parameterized by the dimensionless combination

$$\gamma = \frac{mg}{\hbar^2 n}. \quad (\text{S-9})$$

In the absence of coupling, the condensates can be described within the bosonization framework by the Hamiltonians

$$H_j = \frac{\hbar c}{2} \int dx \left\{ \frac{\pi}{K} \Pi_j(x)^2 + \frac{K}{\pi} [\partial_x \varphi_j(x)]^2 \right\}, \quad (\text{S-10})$$

where  $[\varphi_j(x), \Pi_j(x')] = i\delta(x-x')$ . The speed of sound,  $c$ , and the Luttinger parameter  $K$  can be computed from the exact Bethe Ansatz solution of the model. The asymptotic expansions for small and large couplings are

$$K \approx \frac{\pi}{\sqrt{\gamma}} \left( 1 - \frac{\sqrt{\gamma}}{2\pi} \right)^{-1/2} \approx \hbar\pi \sqrt{\frac{n}{mg}}, \quad c \approx \sqrt{\frac{ng}{m}} \quad \text{for } \gamma \lesssim 10, \quad (\text{S-11a})$$

$$K \approx (1 + 4/\gamma), \quad c \approx \hbar\pi n/m \quad \text{for } \gamma \gg 1. \quad (\text{S-11b})$$

Due to Galilean invariance,  $cK = \hbar n\pi/m$  holds for all  $\gamma$ . The density fluctuations are suppressed at wavelengths smaller than the healing length which is also used as a short distance cutoff. For small  $\gamma$  it is

$$\xi_h = 1/(n\sqrt{\gamma}) = \hbar/\sqrt{mgn} \approx \hbar/mc, \quad (\text{S-12})$$

while at strong coupling  $\xi_h \approx 1/n$ . The coupling between the condensates is captured by the term  $2\Delta \cos(\varphi_1 - \varphi_2)$ , where  $\Delta \approx \hbar J n$  for weak coupling, but it can be renormalized at strong interactions. It is convenient to introduce the total and relative phase  $\varphi_\pm = \varphi_1 \pm \varphi_2$  and  $\Pi_\pm = (\Pi_1 \pm \Pi_2)/2$  in terms of which the two Hamiltonians decouple. For the phase difference we obtain the sine–Gordon Hamiltonian [32]

$$H_- = \frac{\hbar c}{2} \int dx \left[ \frac{2\pi}{K} \Pi_-(x)^2 + \frac{K}{2\pi} [\partial_x \varphi_-(x)]^2 \right] - \int dx 2\Delta \cos[\varphi_-(x)]. \quad (\text{S-13})$$

### Fluctuations of the phase

We are interested in the fluctuations of  $\varphi_-$  around the minima of the cosine potential. We will calculate this in the harmonic approximation, i.e. by expanding the cosine up to quadratic order which yields

$$H_- \approx \frac{\hbar c}{2} \int dx \left[ \frac{2\pi}{K} \Pi_-(x)^2 + \frac{K}{2\pi} [\partial_x \varphi_-(x)]^2 + \frac{2\Delta}{\hbar c} \varphi_-(x)^2 \right], \quad (\text{S-14})$$

a free massive boson theory with mass gap

$$m_0 = \sqrt{\frac{4\Delta\hbar\pi}{c^3 K}} = \sqrt{\frac{4\Delta m}{nc^2}}. \quad (\text{S-15})$$

The mode expansion of the fields are

$$\varphi(x) = \sqrt{\frac{\pi c}{K}} \int \frac{dp}{2\pi} \frac{1}{\sqrt{\omega(p)}} \left[ b_p e^{ipx/\hbar} + b_p^\dagger e^{-ipx/\hbar} \right], \quad (\text{S-16})$$

$$\Pi(x) = -\frac{i}{2\hbar} \sqrt{\frac{K}{\pi c}} \int \frac{dp}{2\pi} \sqrt{\omega(p)} \left[ b_p e^{ipx/\hbar} - b_p^\dagger e^{-ipx/\hbar} \right] \quad (\text{S-17})$$

with  $\omega(p) = \sqrt{p^2 c^2 + m_0^2 c^4}$  and  $[b_p, b_{p'}^\dagger] = 2\pi\delta(p - p')$ .

The finite temperature equal time correlation function of the phase is

$$\langle \varphi(x)\varphi(x') \rangle_T = \frac{\pi c}{K} \int \frac{dp}{2\pi} \frac{1}{\omega(p)} e^{ip(x-x')/\hbar} \coth(\beta\omega(p)/2), \quad (\text{S-18})$$

where we used  $\langle b_p^\dagger b_{p'} \rangle = 2\pi\delta(p - p') f_T(p)$  with  $f_T(p) = 1/(e^{\omega(p)/(k_B T)} - 1)$  the thermal Bose–Einstein distribution and  $\beta = 1/(k_B T)$ .

### Quantum fluctuations ( $T = 0$ )

At zero temperature the integral can be evaluated in closed form,

$$\langle \varphi(x)\varphi(x') \rangle_{T=0} = \frac{\pi c}{K} \int \frac{dp}{2\pi} \frac{1}{\omega(p)} e^{ip(x-x')/\hbar} = \frac{1}{K} K_0[m_0 c |x - x'|/\hbar] = \frac{1}{K} K_0\left(\frac{\Delta x}{l_\Delta}\right), \quad (\text{S-19})$$

where  $\Delta x = |x - x'|$ ,  $K_0(z)$  is the modified Bessel function of the second kind and

$$l_\Delta \equiv \frac{\hbar}{m_0 c} = \sqrt{\frac{\hbar^2 n}{4m\Delta}} \quad (\text{S-20})$$

is the Compton wavelength associated with the mass  $m_0$  which physically corresponds to the “healing length of the relative phase”. For small separation

$$\langle \varphi(x)\varphi(x') \rangle_{T=0} = -\frac{1}{K} \left\{ \log\left(\frac{\Delta x}{2l_\Delta}\right) \left[ 1 + \left(\frac{\Delta x}{2l_\Delta}\right)^2 \right] + \gamma_E \right\} + \mathcal{O}\left[\left(\frac{\Delta x}{l_\Delta}\right)^2\right], \quad (\text{S-21})$$

so it is logarithmically divergent ( $\gamma_E$  is the Euler–Mascheroni constant). By introducing a minimum distance  $\alpha$  we obtain

$$\langle \varphi^2 \rangle_{T=0} \approx -\frac{1}{K} \left[ \log\left(\frac{\alpha}{2l_\Delta}\right) + \gamma_E \right]. \quad (\text{S-22})$$

For e.g.  $l_\Delta/\alpha \approx 10$ ,  $\langle \varphi^2 \rangle_{T=0} \approx 2.4/K$ . As  $K > 1$ , this means that the quantum fluctuation of the phase satisfies  $\Delta\varphi \lesssim 1.5$  and remains small compared to  $2\pi$ , so the approximation of the cosine by a quadratic potential is justified.

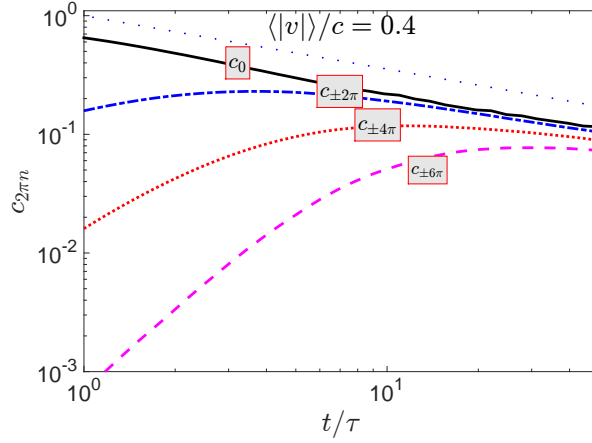


FIG. S-5. (Color online) Time dependence of the weights  $c_{2\pi n}$  defined in Eq. (5) in the main text represented on a logarithmic scale. The dotted blue line represents the expected  $\sim \sqrt{\tau/t}$  dependence corresponding to diffusive behavior in the large time limit.

### Thermal fluctuations (low temperature)

Let us now compute the correlation function focusing on the low temperature limit, i.e. when  $k_B T \ll m_0 c^2$ . The thermal contribution is given by the expression

$$\langle \varphi(x)\varphi(x') \rangle_{\text{therm}} = \frac{\pi c}{K} \int \frac{dp}{2\pi} \frac{1}{\omega(p)} e^{ip(x-x')/\hbar} (\coth(\beta\omega(p)/2) - 1), \quad (\text{S-23})$$

which is perfectly well-behaved for large  $p$ . Expanding the hyperbolic cotangent in powers of  $e^{-\beta\omega(p)}$ , changing the momentum integration variable to relativistic rapidity, and shifting the integration contour we arrive at

$$\langle \varphi(x)\varphi(x') \rangle_{\text{therm}} = \frac{2}{K} \sum_{n=1}^{\infty} K_0 \left( \sqrt{(n\pi q/2K)^2 + (\Delta x/l_\Delta)^2} \right), \quad (\text{S-24})$$

where

$$q \equiv \frac{\lambda_T}{l_\Delta} = \frac{2K}{\pi} \frac{m_0 c^2}{k_B T} \quad (\text{S-25})$$

is the ratio of the thermal phase coherence length  $\lambda_T = 2\hbar^2 n/(mk_B T)$  and  $l_\Delta$ . For the fluctuations of  $\varphi$  this implies

$$\langle \varphi^2 \rangle_T = \langle \varphi^2 \rangle_{T=0} + \langle \varphi^2 \rangle_{\text{therm}} \approx \frac{1}{K} \left[ -\log \left( \frac{\alpha}{2l_\Delta} \right) - \gamma_E + 2 \sum_{n=1}^{\infty} K_0 \left( n \frac{\pi q}{2K} \right) \right]. \quad (\text{S-26})$$

In the low temperature limit  $\pi q/(2K) \gg 1$  so we can expand the Bessel functions:

$$K_0 \left( n \frac{\pi q}{2K} \right) = \sqrt{\frac{K}{nq}} e^{-n\pi q/(2K)} \left( 1 - \frac{K}{4\pi nq} + \mathcal{O} \left[ \left( \frac{K}{\pi nq} \right)^2 \right] \right). \quad (\text{S-27})$$

Each term in the sum in Eq. (S-26) is exponentially suppressed with respect to the previous one, so we can truncate the series at the first term, leading to

$$\langle \varphi^2 \rangle_T \approx \frac{1}{K} \left( -\log \left( \frac{\alpha}{2l_\Delta} \right) - \gamma_E + 2\sqrt{\frac{K}{q}} e^{-m_0 c^2/(k_B T)} \right). \quad (\text{S-28})$$

The calculation is consistent if  $\langle \varphi^2 \rangle_T \ll 1$  so the approximation of the cosine by a quadratic potential is justified.

With the the results for the fluctuations at hand we can dress up the phase distribution (Eq.(5) in the main text) by broadening the  $\delta$ -peaks accordingly. For completeness, we also represent in Fig. S-5 the coefficients  $c_{2\pi n}$  on a log-log scale which shows a decay  $\sim 1/\sqrt{(t/\tau)}$  further supporting the diffusive behavior for the propagation of the phase, as discussed in the main body of the paper.

### S-matrix of the sine-Gordon model

The 2-particle S-matrix describing the scattering of two kinks is exactly known [42]. The energy and momentum of the incoming and outgoing particles are conveniently parameterized in terms of the relativistic rapidity as  $E = mc^2 \cosh \theta$ ,  $p = mc \sinh \theta$ . The 2-particle S-matrix is given by a four by four matrix in the basis  $|+\rangle, |+\rangle, |-\rangle, |-\rangle$ :

$$S = \begin{pmatrix} S & & & \\ & S_T & S_R & \\ & S_R & S_T & \\ & & & S \end{pmatrix}, \quad (\text{S-29})$$

where due to relativistic invariance all entries depend only on the relative rapidity  $\theta = \theta_1 - \theta_2$  of the two incoming kinks. Here  $S_T$  is the amplitude of transmission and  $S_R$  is the amplitude of reflection. The term  $S$  accounts for the phase picked up by the wave function upon scattering of two kinks of the same charge:

$$S(\theta) = -\exp \left\{ -i \int \frac{dt}{t} \frac{\sinh \frac{t(\pi-\xi)}{2}}{\sinh \frac{\xi t}{2} \cosh \frac{\pi t}{2}} \sin(\theta t) \right\}, \quad (\text{S-30})$$

where

$$\xi = \frac{\pi}{4K-1}. \quad (\text{S-31})$$

The transmission and reflection factors are given by

$$S_T(\theta) = \frac{\sinh \frac{\pi\theta}{\xi}}{\sinh \frac{\pi(i\pi-\theta)}{\xi}} S(\theta), \quad (\text{S-32})$$

$$S_R(\theta) = i \frac{\sin \frac{\pi^2}{\xi}}{\sinh \frac{\pi(i\pi-\theta)}{\xi}} S(\theta). \quad (\text{S-33})$$

and they satisfy  $|S_T|^2 + |S_R|^2 = 1$ . For small  $\theta$  they behave as  $|S_T|^2 \propto \theta^2$ ,  $|S_R|^2 \propto 1 - \theta^2$ , thus at small rapidities the scattering of kinks of opposite charges is almost purely reflective.

### Details of the numerical algorithm

In this section we discuss in more detail the numerical algorithm which is a combination of Monte Carlo (MC) sampling of classical trajectories for the soliton-antisoliton pairs and a propagation in time of the initial wave function  $|\Psi_{\text{orb}}(\mathbf{x}, t)\rangle$  using the Time-Evolving Block Decimation (TEBD) approach. The process can be divided into three main steps as follows:

(1) *Generation of classical kink configurations*– For a given concentration of pairs, we randomly generate their positions at  $t = 0$ . The kink velocities are generated from a given velocity distribution [50]. Then we construct the kink configuration (one such configuration is presented in Fig. S-6(a)) which is a space-time diagram in  $(x, t)$  coordinates that displays the classical trajectories of the kinks. We have to keep in mind that at  $t = 0$  two kinks that form a pair start to move in opposite directions with equal velocities. In this representation the collision of two kinks corresponds to the intersection of two lines. When constructing the kink configuration we index all the intersection points in the space-time coordinates  $(x_I, t_I)$  as well as the corresponding lines. These coordinates are then ordered chronologically. In this way we completely characterize the orbital motion of the kinks, which corresponds to the construction or the orbital part of the wave function  $|\Psi_{\text{orb}}(\mathbf{x}, t)\rangle$  in Eq. (2b). Furthermore (although not displayed in Fig. S-6(a)) we impose hard wall boundary conditions such that a kink is perfectly reflected off the walls.

(2) *Construction of the effective spin model*– Quantum effects become relevant only at collision times and they do not affect the orbital motion of the quasiparticles, which allows us to factorize the wave function as in Eq. (2) in the main body of the paper. To be able to propagate the initial wave function we need to map the dynamics of the spins to an effective spin model. We do that by constructing first zig-zag kink configuration, which consists of relabeling the lines according to Fig. S-6(b). In this way, the lines are ordered from left to right at any time instance  $t$  but, more

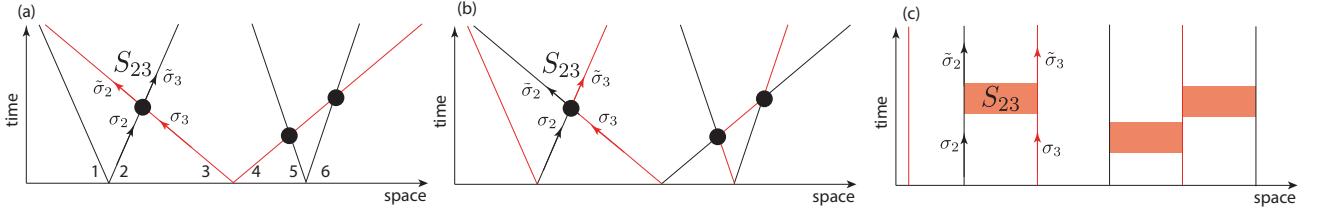


FIG. S-6. (Color online) (a) A typical kink configuration with soliton-antisoliton pairs. Their space-time evolution is described by pairs of straight lines. Different lines are plotted with different colors. (b) Reindexing the lines after each collision. The quasiparticle trajectories have now zig-zagged shapes indicated by the colors. With this labeling the collisions always take place between neighboring quasiparticles. (c) Propagation of the TEBD solution in the charge sector of the wave function. When two lines intersect in (b), the effective spin chain of the charge sector is acted on by the unitary evolution operator given by the corresponding S-matrix.

importantly, in this representation only neighboring lines intersect. Furthermore, each line  $j$  carries a “spin”  $\sigma_j$ . The intersections of classical lines corresponds to a scattering event of the two spins carried by the lines. This is a quantum mechanically process that is fully described in terms of the S-matrix, so at this point the model Hamiltonian is not relevant as all the necessary information that we need is encoded in the two-body S-matrix.

(3) *Time evolution of the wave function*– The mapping of the zig-zag kink configuration to the effective spin chain model is displayed in Fig. S-6(c). Here the square regions indicate the interaction between two neighboring spins. Basically, the spin chain is frozen in time in between collisions and the time evolution takes place only when pairs of spins are scattered at the collision times. This picture allows us to use the TEBD algorithm [10, 11] and propagate the initial wave function. The  $t = 0$  wave function  $|\chi(\boldsymbol{\sigma}, t = 0)\rangle$  given in Eq. (3) is first organised as an MPS state which is then evolved in time. The full time evolution operator  $U(t)$  is the chronological product of unitary two-body S-matrix operators that scatter pairs of quasiparticles only at the intersection times  $t_I$ . Furthermore, the TEBD framework allows us to compute different physical quantities [11]. For example, to compute the time evolution of the entanglement entropy, we first evolve the MPS state up to the desired time  $t$ , bipartition the state using the Schmidt decomposition and then compute the entanglement entropy in the usual way [11].

What we have described so far is the evolution of a single kink configuration. To compute the averages discussed in the main body of the paper, we sample in general  $\sim 10^5$  such configurations and average over their positions and velocity distribution.